ACS Biomaterials SCIENCE & ENGINEERING

pubs.acs.org/journal/abseba

Article

Silicon Nanoneedle Patches for Painless, Sustained Treatment of Macular Degeneration

Van Phuc Nguyen, Jinheon Jeong, Josh Zhe, Mi Zheng, Junsang Lee, Khoi Tran, Zhuying Wei, Chi Hwan Lee,* and Yannis M. Paulus*

Cite This: *ACS Biomater. Sci. Eng.* 2026, 12, 1269−1285

Read Online

ACCESS | Metrics & More | Article Recommendations | Supporting Information

ABSTRACT: Choroidal neovascularization (CNV) represents a major cause of vision loss in various retinal diseases such as age-related macular degeneration (AMD). Current treatment involves frequent, often monthly, eye injections. The development of minimally invasive, long-term, painless, and effective ocular drug delivery systems is crucial for advancing the treatment of AMD. This study explores a novel method that integrates controllably bioresorbable silicon nanoneedles loaded with bevacizumab (Si NNs-Bev) on a tear-soluble subconjunctival patch for sustained, 1 year ocular drug delivery. The Si NNs-Bev embed into the sclera in a minimally invasive manner, undergoing controlled degradation over one year. This approach facilitates the sustained release of therapeutic agents, enhancing treatment efficacy and reducing treatment burden. Si NNs-Bev for the treatment of CNV are validated in a rabbit model of AMD. The SiNN-Bev patch achieved a sustained therapeutic effect on CNV regression, with a mean reduction of 82% by 4 months that is persistent for at least 1 year with minimal recurrence, which is consistent with the localized drug delivery mechanism facilitated by the transscleral microneedles. These preliminary findings underscore the potential of SiNNs as a platform technology for long-term, sustained ocular therapeutics.

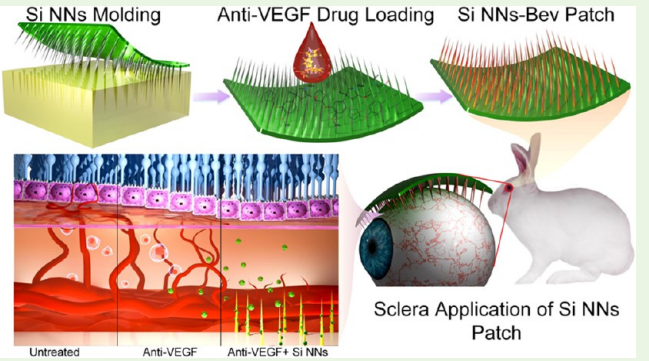

KEYWORDS: *bioresorbable silicon nanoneedles, age-related macular degeneration, ocular drug delivery system, anti-VEGF, photoacoustic microscopy, optical coherence tomography*

Eye diseases affecting the posterior segment can be sight-threatening and require long-term, invasive treatment. How to deliver drugs to the posterior segment efficiently and with less invasive techniques has attracted the attention of many researchers. The three most common methods of drug delivery to the posterior segment are systemic administration, topical application, and intravitreal injection. Systemic administration, such as oral administration and intravenous injection, usually requires a large dose to achieve an effective drug concentration in the eye, which can cause toxicity to other organs and lead to complications. Topical eye drops are a common method for ocular drug delivery. While they are easy to administer, their efficacy is limited by human reflexes such as blinking or tearing. The barriers of the eye result in less than 5% of the drug reaching its desired target, with the rest being washed away.[1−4] Even drugs that are not washed away can be absorbed by the capillaries in the lacrimal sac and conjunctiva, which further limits the amount of drug that reaches the desired target inside the eye.[5,6] Intravitreal injections are a viable alternative; however, they are off putting for many patients due to their invasive nature, risks including risk of eye infection and blindness, and frequent administration requiring the need for a doctor's visit for each treatment. In consequence of these considerations, researchers have focused their attention on less invasive treatments. Microneedle array dissolvable contact lenses have been tested as a method of drug delivery that is less invasive than intravitreal injections, but more effective and sustained than topical eye drops. However, the submillimeter size of microneedles can cause pain to the highly sensitive cornea along with corneal damage.[7] With recent developments, the size of needles has been shrunk to a 250 μm diameter at the base and made from biodegradable materials that allow for both fast and slow drug release.[8−11]

Silicon nanoneedle arrays (Si NNs) are an emerging, modern method of efficiently delivering drugs. Dissolvable Si NNs allow for painless and noninvasive treatment of ocular diseases as well as slow and extended release of medications in the eye, allowing for less frequent application. Chronic ocular

Received: October 13, 2025
Revised: January 13, 2026
Accepted: January 14, 2026
Published: January 19, 2026

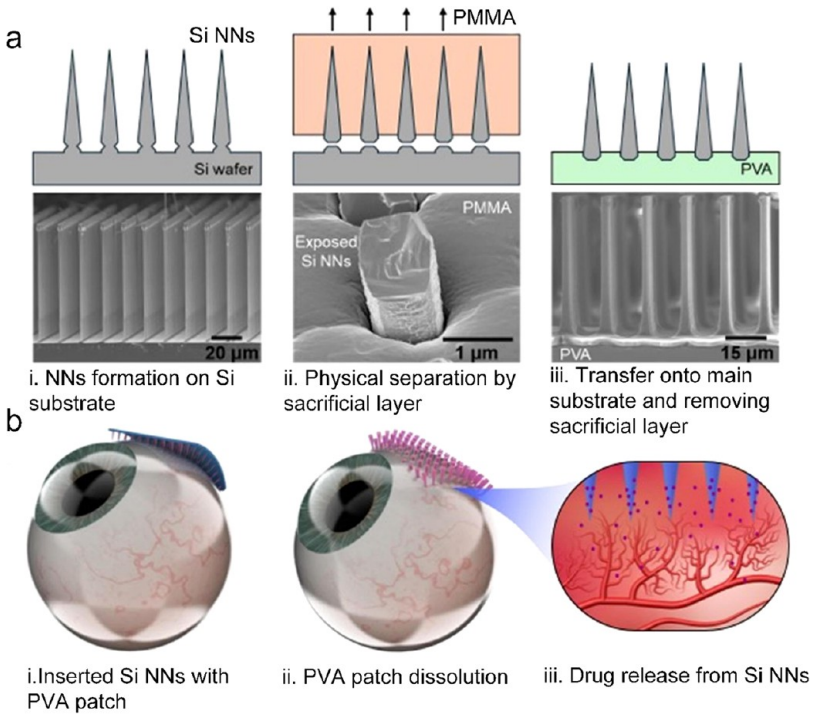

Figure 1. Si NNs fabrication and application in the retina. (a) Schematic illustrations (top) and SEM images (bottom) for the process flow regarding the physical transfer of the as-prepared Si NNs from the Si wafer to a biodegradable film. (b) Schematic illustration of working principles for the drug delivery process.

disease such as macular degeneration, diabetic retinopathy, and corneal neovascularization may benefit from long-term sustained release of drug therapy.[12] Long-term sustained release can be achieved using passivation layers from compounds such as aluminum oxide to slow the degradation rate of the Si NNs.[12] Silicon itself also has a much slower degradation speed than many other common needle composites. In physiological conditions, Si NNs degrade at a rate of <20 nm/day while other composites such as such as poly(lactic-*co*-glycolic) acid (PLGA) and methacrylate hyaluronic acid (MeHA) degrade at rates of 24 to 120 μm/day.[12−14] The initial contact lens dissolves within minutes once inserted onto the eye, leaving behind embedded nanoneedles that slowly dissolve and release their drug payload. The nanoscale size of the needles allows for no lasting damage to the cornea and a painless application. While Park et al. have demonstrated the feasibility of silicon-based microneedles for ocular delivery, our study uniquely integrates controllably bioresorbable Si NNs with a tear-soluble subconjunctival patch for painless, self-adhering application and year-long sustained release.[12] This configuration eliminates the need for injections or external applicators and provides, to our knowledge, the first long-term (12-month) *in vivo* validation of anti-VEGF efficacy using bioresorbable Si NNs.

CNV is a common complication of many diseases, including wet age-related macular degeneration (AMD) and pathologic myopia. The development of effective therapeutic interventions to mitigate CNV progression and promote regression is imperative in preserving visual function. While antivascular endothelial growth factor (anti-VEGF) agents have revolutionized CNV management, longitudinal monitoring of treatment response and structural changes remains essential for optimizing patient outcomes. While many anti-VEGF drugs have been approved for CNV treatment, the methods of delivering the drug payload are not optimal.[15] Regorafenib, a multikinase inhibitor, was studied in a phase 2 clinical trial as a potential topical treatment of neovascular AMD. However, by week 12, 41% of the 51 subjects developed adverse treatment emergent events which required intravitreal ranibizumab rescue. The most likely cause was insufficient drug delivery to the posterior segment of the eye.[16] Due to the inadequacy of other available strategies, intravitreal injection is still the main way to deliver anti-VEGF drugs to the back of the eye.

Anti-VEGF biologics such as ranibizumab and bevacizumab have a short half-life and require monthly or bimonthly injections in order to maintain their treatment efficacy.[17−21] Unfortunately, monthly intravitreal injections are not well tolerated by patients due to the invasive nature of the technique, the cost, and the risk, including the risk of eye infection (endophthalmitis), which can result in blindness.[22,23] The efficacy of intravitreal injections is severely limited by the presence of the inner limiting membrane (ILM), a physical barrier between the vitreous and the retina. Since the ILM is not essential in the adult eye and Müller cell reparation of the ILM is extremely slow, many methods have been created to disrupt the ILM through surgical peeling, enzymatic digestion, or photoablation.[24−27] The ILM increases in thickness with age, potentially affecting the efficacy of intravitreal injections in older patients which are affected by AMD.[28] The ILM can be avoided through subretinal injections; however, these are invasive and burdensome for patients as they may even require vitrectomy surgery and general anesthesia.[29] Importantly, even if the ILM is bypassed via subretinal injection, a bolus delivery lacks the sustained-release kinetics required for long-term treatment. The SiNN platform uniquely combines the circumvention of the ILM barrier via a transscleral route, and the year-long sustained release achieved through the gradual degradation of the nanoneedles, a synergistic

https://doi.org/10.1021/acsbiomaterials.5c01783
ACS Biomater. Sci. Eng. 2026, 12, 1269−1285

advantage that cannot be replicated by standard subretinal or intravitreal bolus injections. Our therapeutic strategy is based on the hypothesis that the SiNNs enable sustained, localized transscleral delivery. By utilizing nanoneedles that embed in the sclera and continuously release the drug directly beneath the outer diffusion barriers, we aim to minimize systemic exposure and maximize the therapeutic concentration delivered locally to the CNV. This article explores the efficacy of a novel Si NNs on delivering bevacizumab (Avastin) to treat CNV in a long-term, sustained manner.

RESULTS AND DISCUSSIONS

Soluble Si NNs Patch Fabrication and Characteristics

Figure 1a illustrates the fabrication flow of a biodegradable ocular drug delivery patch using Si NNs on a Si wafer, as evidenced by the scanning electron microscopy (SEM) images. The process begins with the cleaning of a p-type bulk Si wafer (525 μm thick; 0 to 100 Ω·cm) using a sulfuric peroxide mixture (SPM; H_2SO_4/H_2O_2 = 4:1) and diluted hydrofluoric acid (HF), to remove organic contaminants and native oxide layers. A photolithographic procedure defines a microscale pattern, which is then transformed into vertically aligned Si micropillars (base diameter, 2 μm; height, 75 μm) through deep reactive ion etching (DRIE). These pillars undergo an alternate deposition and vertical etching process, followed by additional isotropic etching to create an undercut at the base. Subsequent oxygen (O_2) plasma and SPM treatments eliminate the passivation layer and photoresist residues. The pillars are then downscaled to Si NNs by immersing in a 15 wt % potassium hydroxide (KOH) solution at room temperature. Nanopores are introduced on the Si NNs surface via metal-assisted chemical etching (MACE) in a solution of 20 mM silver nitrate ($AgNO_3$) and 49% HF, enhancing drug loading capacity.[12] After removing the residual Ag with an etchant, the Si NNs are coated with a 3 nm aluminum oxide (Al_2O_3) layer by atomic layer deposition (ALD), forming the Si NNs array depicted on the left side of Figure 1a.

The integration of the patch with the Si NNs for drug delivery involves coating the Si NNs with a 200 μm poly(methyl methacrylate) (PMMA) film via spin-casting on the Si wafer, followed by annealing at 80 °C for 2 h. The PMMA layer is mechanically peeled off, uncovering the Si NNs base with an air gap formed by surface tension during annealing (Figure 1a, middle).[30] The exposed PMMA is then coated with a 2 wt % poly(vinyl alcohol) (PVA; molecular weight = 31,000) solution, with the process repeatable to control patch thickness, adding approximately 10 μm per layer. After coating, the PMMA is dissolved in acetone at 70 °C for 4 h, followed by rinsing and ultraviolet (UV) sterilization (Figure 1a, right). The Si NNs fabrication process leverages wafer-scale photolithography and etching techniques that are compatible with standard semiconductor manufacturing, supporting scalability and batch-to-batch reproducibility. The integration of Si NNs onto tear-soluble films via transfer printing has also been demonstrated on large-area substrates.

The fabrication of the Si NNs leverages wafer-scale photolithography, deep reactive ion etching, metal-assisted chemical etching, and atomic layer deposition processes that are fully compatible with standard semiconductor manufacturing, supporting scalability and batch-to-batch reproducibility. The nanoneedle arrays were mechanically robust during transfer printing, sterilization, and handling, with no observable structural damage or delamination. The tear-soluble subconjunctival patch format enables reproducible user-applied placement without the need for specialized applicators, and consistent dissolution and nanoneedle retention within 1 min were observed. Sterilization using ethanol soaking and ultraviolet exposure did not adversely affect device integrity or therapeutic efficacy. These results collectively support the translational feasibility of the Si NNs platform.

To enable therapeutic delivery, Bevacizumab was covalently immobilized onto the surface of the Si NNs using silane chemistry involving 3-triethoxysilylpropyl succinic anhydride (TESPSA), forming stable amide bonds between the NNs surface and the protein. This chemical strategy ensures strong retention of the drug during handling and implantation, while allowing sustained release upon gradual degradation of the nanoneedles. The Si NNs feature nanoporous surfaces that increase drug binding capacity and enhance loading stability. The nanoporous surface morphology of the Si NNs is confirmed by representative SEM images shown in Supporting Information Figure S1. The drug loading capacity of the Si NNs used in this study has been previously quantified to range from 1 to 17 μg, depending on surface porosity and needle length. The *in vitro* degradation rate of Si NNs has been previously measured to range from 3.5 to 16.6 nm/day depending on porosity, and as low as ∼0.05 nm/day with a 3 nm Al_2O_3 passivation layer. While the present study focuses on *in vivo* therapeutic validation, prior work using the same Si NNs configuration demonstrated long-term, controlled protein release.[12] Specifically, fluorescently labeled IgG (used as a surrogate for Bevacizumab) showed sustained release from the nanoneedles over a period of 55 days under simulated physiological conditions. The release profile exhibited a biphasic pattern with an initial burst from the tear-soluble layer and extended release from the nanoneedle surface. Importantly, ELISA confirmed that the bioactivity of the released protein was preserved throughout the release period. These findings validate the Si NNs platform's suitability for sustained ocular drug delivery. The structural and functional stability of antibodies loaded onto Si NNs has been previously validated using ELISA and SDS-PAGE, which confirmed retention of molecular integrity and bioactivity after fabrication and release.[12] While sustained therapeutic efficacy was validated through functional imaging and histological analyses over 12 months, a key limitation is the absence of direct, mechanistic evidence confirming the hypothesized drug distribution pathway. Future studies could incorporate pharmacokinetic measurements to further confirm the long-term drug presence and release profile.

Figure 1b presents the operational principle of the patch. When applied to the eye, the Si NNs embed into the sclera layer of the retina (Figure 1b, left). The patch, made of tear-soluble materials, dissolves within a minute, releasing anti-inflammatory or other desired ocular drugs rapidly (Figure 1b, middle). The Si NNs then dissolve slowly in sclera, typically over many months, converting into silicic acid and hydrogen through hydrolysis in the tear fluid.[31−33] This enables a sustained, extended local release of the drugs.

In Vivo Si NNs Patch Dissolution Monitoring Using OCT Imaging

To evaluate the real-time interaction between the Si NNs and the ocular tissue, we performed *in vivo* OCT monitoring before, during, and after patch application (Figure S2).

https://doi.org/10.1021/acsbiomaterials.5c01783
ACS Biomater. Sci. Eng. 2026, 12, 1269−1285

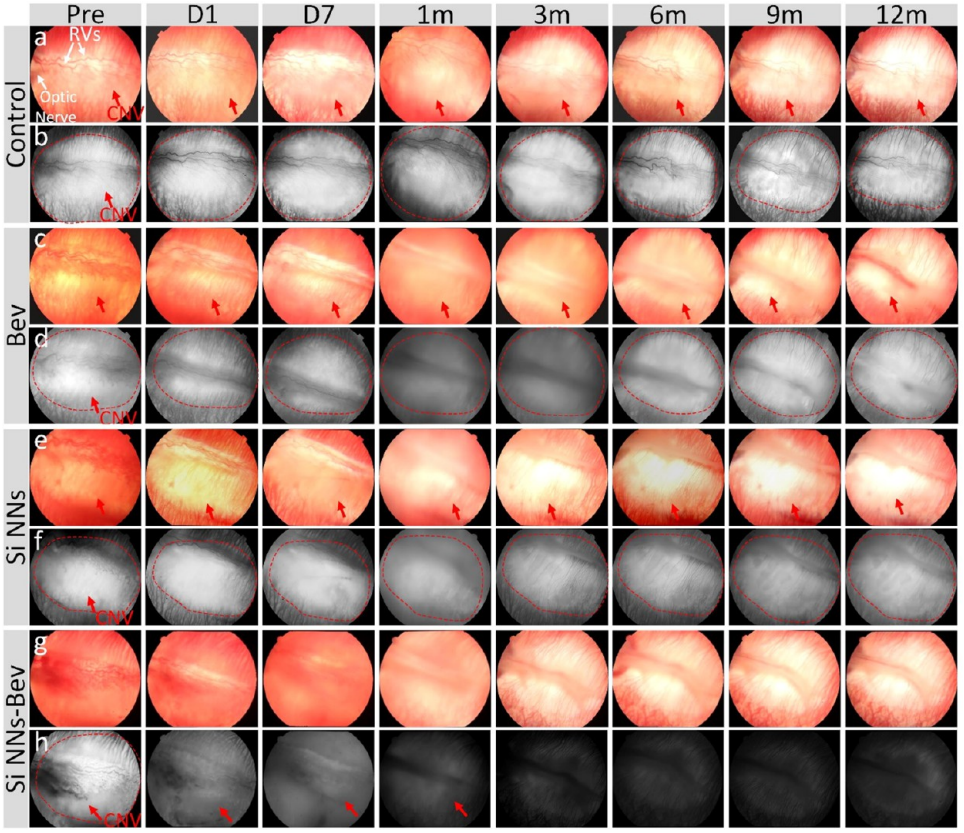

Figure 2. Longitudinal visualization of CNV progression following treatment with Si NNs: (a, c, e, g) Color fundus photography (CFP) images showing CNV before and after treatment with Si NNs at various time points in the control group (a), Bev-only injection group (c), Si NNs without Bev group (e) and the Si NNs-Bev treated group (g). These images depict the morphology of retinal vessels (RVs), optic nerve, and newly developed CNV. Morphology of the choroidal vessels were lightly changed from month 3 post-treatment, indicated by increased brightness. Persistent CNV was observed in the control (a) and Si NNs without Bev (e) groups, while partial regression followed by recurrence was seen in the Bev-only group (c). In contrast, the Si NNs-Bev group (g) show CNV lesions gradually regressed with minimal recurrence up to 12 months. (b, d, f, h) Corresponding fluorescein angiography (FA) images of the same groups, showing leakage areas from CNV: control (b), Bev-only injection group (d), Si NNs without Bev (f) and Si NNs-Bev treatment group (h). The control (b) and Si NNs without Bev (f) groups showed persistent CNV leakage, whereas the Bev-only group (d) showed early reduction in leakage followed by recurrence starting at month 4. The Si NNs-Bev group (h) showed reduced fluorescence intensity starting from month 1 post-treatment and sustained suppression of leakage through 12 months. (N = 3 per group).

Baseline imaging clearly delineated the stratified structure of the sclera (Figure S2a). Upon application, the Si NN layer was observed successfully penetrating the scleral surface (indicated by dotted lines in Figure S2b,c). Due to the bioresorbable nature of the porous silicon, the nanoneedle layer underwent rapid dissolution, becoming significantly attenuated by 30 s and completely undetectable within 60 s postapplication (Figure S2d). This confirms the rapid degradation kinetics of the Si NNs within the interstitial fluid of the sclera. Importantly, follow-up imaging at day 3 post-treatment (Figure S2e) revealed a preserved scleral architecture with no signs of structural destruction, localized edema, or inflammatory thickening, suggesting that the gentle embedding and subsequent dissolution of the needles do not compromise tissue integrity.

In Vivo Color Fundus and Fluorescein Angiography Visualization

In this study, we investigated the efficacy of Si NNs conjugated with bevacizumab (Si NNs-Bev) in the treatment of CNV in rabbits. The treatment outcomes were visualized using color fundus and fluorescein angiography (FA) over a 12-month period. The control group without Si NNs-Bev treatment (Figure 2a,b) exhibited progressive growth of CNV lesions over the same duration, emphasizing the effectiveness of the Si NNs-Bev treatment in halting CNV progression. We observed that CNV treated with Bev alone (Figure 2c,d, Supporting Information Figure S3) initially showed a gradual decrease in size by day 3 post-treatment. However, CNV began to regrow from day 7, with a subsequent reduction observed between 1 and 3 months. Notably, CNV recurred starting from month 4 and stabilized by 12 months (Supporting Information Figure S3). With the with Si NNs without conjugation with Bev treatment group, the CNV regression was not significantly reduced over time (Figure 2e,f, Supporting Information Figure S4). In contrast, upon subconjunctival treatment with the Si NNs-Bev patch, CNV regression was evident as early as 1-month post-treatment, as observed on color fundus photography (Figure 2g and Supporting Information Figure S5a,c) and FA imaging (Figure 2h, and Supporting Information Figures S5b,d). Remarkably, CNV lesions nearly completely resolved by 4 months, with minimal recurrence observed for up to 12 months post-treatment. This sustained absence of CNV highlights the long-term efficacy of the Si NNs-Bev patch in inhibiting pathological angiogenesis within the choroid. These findings underscore the therapeutic potential of Si NNs-

https://doi.org/10.1021/acsbiomaterials.5c01783
ACS Biomater. Sci. Eng. 2026, 12, 1269−1285

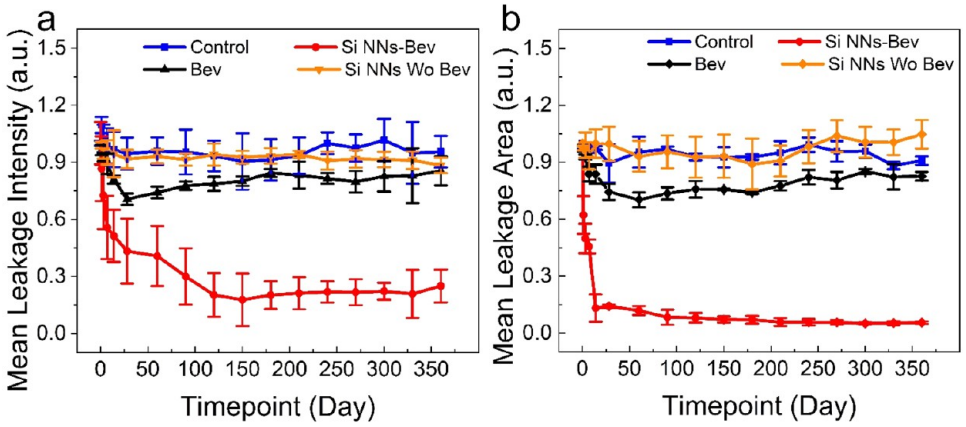

Figure 3. Quantification of normalized mean fluorescent leakage intensity and area in rabbits. (a) Graph showing normalized mean fluorescent leakage intensity measured before and up to 12 months after treatment with Si NNs. The data indicate a significant reduction in fluorescent signal over time in the Si NNs-Bev treated group (red line). In contrast, the control group (blue line) exhibited only a slight decrease in fluorescent intensity. (b) Graph of normalized mean leakage area, demonstrating a decrease in CNV areas within 2 months post-treatment with Si NNs (red line), while the control group showed no significant reduction in CNV area (blue line). Data are presented as Mean ± Standard Deviation ($N = 3$ per group). As this is a pilot study, the interpretation of p-values should be tempered by the small sample size, which limits statistical power and generalizability.

Table 1. Comparative Summary of Outcomes across Treatment Groups

Parameter	Control	Bev-only Injection	Si NNs without Bev	Si NNs-Bev Patch
CNV Regression	No regression	Partial regression; recurrence by 4 months	No regression	~82% reduction by 4–5 months; sustained to 12 months
FA Leakage Intensity	Persistent leakage	Decreased until 2 months; recurrence after 4 months	Persistent leakage	Significantly reduced leakage ($p < 0.001$)
OCT CNV Thickness	No significant change	~20% reduction	~10% reduction	~83% reduction
PAM Vessel Density	No change	~15% reduction	No change	~82% reduction
TUNEL (Apoptosis)	None observed	None observed	None observed	None observed
Immunofluorescence (α-SMA)	9.18% Positive Area	7.45% Positive Area	9.01% Positive Area	1.12% Positive Area
Signs of Inflammation/ Pain	None	None	None	None

Bev as a promising minimally invasive and long-lasting approach for the management of CNV. The sustained therapeutic efficacy observed over the 12-month study period is consistent with a material-governed release mechanism, in which gradual biodegradation of the silicon nanoneedles enables prolonged local presentation of Bevacizumab at the target tissue. Although direct pharmacokinetic quantification of Bevacizumab levels in ocular tissues was not performed in this study, the durable suppression of CNV demonstrated by longitudinal multimodal imaging and histological analyses supports the presence of sustained bioactive drug levels. These results suggest that the long-term efficacy arises from continuous, degradation-mediated drug release rather than transient exposure, while acknowledging that future studies incorporating pharmacokinetic measurements will be required to further validate drug distribution and clearance profiles.

Next, we evaluated the effect of treatment with Si NNs-Bev on mean fluorescein intensity (FLI) quantification and vessel density (VD). The mean fluorescent leakage, indicative of vascular permeability, was quantified over a period of up to 12 months post-treatment. We first performed the segmentation of FA images to isolate the region of developed CNV (Supporting Information Figures S6 and S7). Then, the mean FLI intensity and VD were measured using Matlab. Following treatment with Si NNs-Bev, there was a gradual reduction in mean fluorescent leakage observed from day 1 post-treatment up to 4 months, after which a plateau in reduction was observed (Figure 3a, red line). This sustained decrease in fluorescent leakage suggests the efficacy of Si NNs-Bev in stabilizing vascular permeability and inhibiting abnormal neovascularization. In contrast, the control groups, which did not receive Si NNs-Bev treatment or treated with Si NNs without conjugation with Bev, exhibited mild fluctuations in FLI over the same period that was essentially unchanged from baseline (blue and orange lines). The group treated with Bev alone showed a gradual decrease in FLI over two months, followed by a resurgence in signal (black line). This result confirms that Bev can inhibit CNV temporarily, but the CNV recurs once the anti-VEGF drug effect diminishes. Compared to pretreatment levels, the mean FLI in the treated group showed pronounced decrease with an average reduction of approximately 82% (FLI = 0.18 ± 0.14 (a.u.) for treatment at 5 months vs 1.00 ± 0.11 (a.u.) for pretreatment, $\mathbf{p< 0.001}$, $\mathbf{N= 3}$). Given the small sample size, this result should be interpreted as a strong preliminary finding, not a statistically robust conclusion. In contrast, the control group and treated group with Si NNs without conjugation with Bev showed a reduction of only 5–12% (FLI = 0.90 ± 0.115 (a.u.) for treatment at 5 months vs 1.00 ± 0.01 (a.u.) for pretreatment). In the group treated with Bev alone, the mean FLI decreased

https://doi.org/10.1021/acsbiomaterials.5c01783
ACS Biomater. Sci. Eng. 2026, 12, 1269–1285

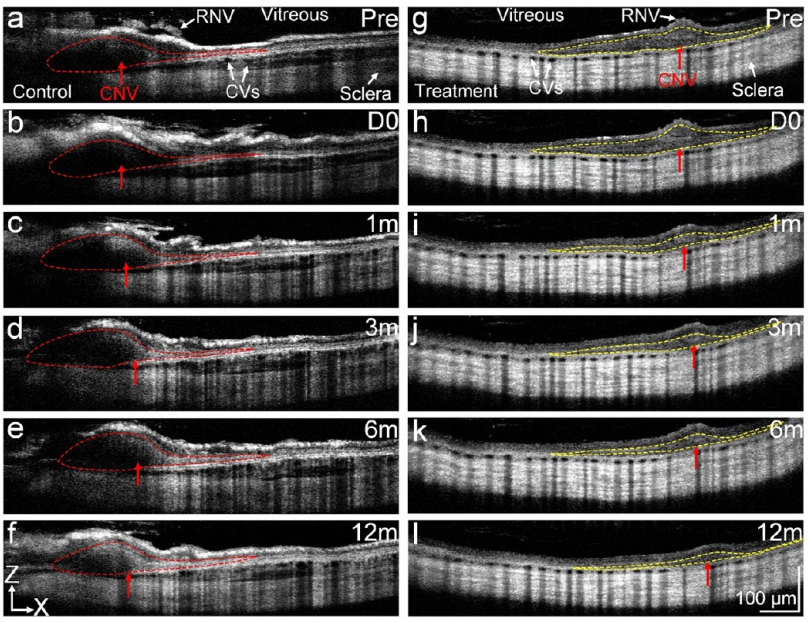

Figure 4. Comparison of CNV lesion areas between the Si NNs-Bev treated group and the control group. (a–f) 2D OCT images from the control group taken before and after treatment at different time points: day 0, and at 1, 3, 6, and 12 months, showing no significant reduction in CNV lesions (indicated by red dotted lines) over the same period, extending up to 12 months. (g–l) 2D SD-OCT images obtained before and after treatment with Si NNs-Bev. The pretreatment OCT images highlight CNV lesions (outlined by yellow dotted lines) and display the vitreous, retinal vessels (RVs), choroidal vessels (CVs), and sclera. The CNV lesions in the treated group gradually decreased over time.

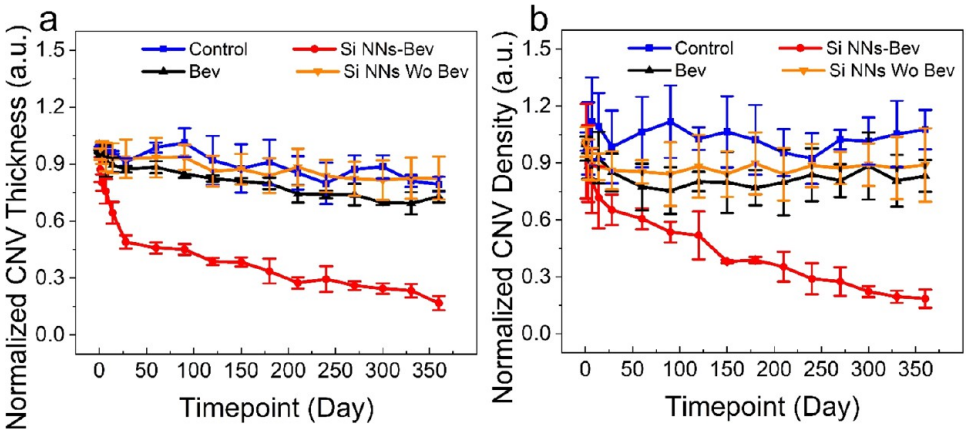

Figure 5. Quantification of normalized CNV thickness and density over time following treatment: (a) Normalized CNV thickness measured using ImageJ. Vascular thickness showed a gradual reduction after treatment with Si NNs-Bev (red line), while the control group, Bev only, and Si NNs without conjugation with Bev displayed a slight decrease in CNV thickness (blue line, black line, and orange line, respectively). (b) Normalized CNV density as a function of treatment time. A significant reduction in CNV density was observed following treatment with Si NNs-Bev, whereas the control group showed minor fluctuations in density. Data are presented as Mean ± Standard Deviation, with $N = 3$, $p = 0.002$ (control vs Si NNs-Bev), $p = 0.2251$ (control vs Bev only), $p = 0.251$ (control vs Si NNs without Bev) at 12 m.

by up to 30% compared to pretreatment levels at 2 months post-treatment (FLI = 0.70 ± 0.03 au at 2 months vs 1.00 ± 0.11 au pretreatment). This reduction in mean fluorescent intensity in the treated group compared to controls provides preliminary evidence of the Si NNs-Bev treatment effect in reducing vascular leakage and retinal edema. Furthermore, analysis of vessel density revealed a similar trend, with a notable decrease observed in the treated group compared to controls (Figure 3b). These results underscore the therapeutic efficacy of Si NNs-Bev in mitigating angiogenesis. To facilitate comparison across groups, a summary of imaging, histological, and safety outcomes is provided in Table 1.

In Vivo OCT Imaging

Figure 4 illustrates representative 2D OCT images obtained pre- and post-treatment at different time points up to 12 months. The control group exhibited persistent CNV lesions post-treatment, as evidenced by OCT imaging (Figure 4g–l), with minimal regression compared to baseline (Figure 4g). Moreover, structural changes in the retina were noted post-CNV induction using subretinal injection with Matrigel and VEGF, consistent with previous reports.[34,35] Specifically, retinal atrophy and loss of retinal layers, including the outer nuclear layer and photoreceptors, was evident. In the group treated with Si NNs-Bev, OCT images obtained before the treatment (Figure 4a) exhibits clearly the margin and location

https://doi.org/10.1021/acsbiomaterials.5c01783
ACS Biomater. Sci. Eng. 2026, 12, 1269–1285

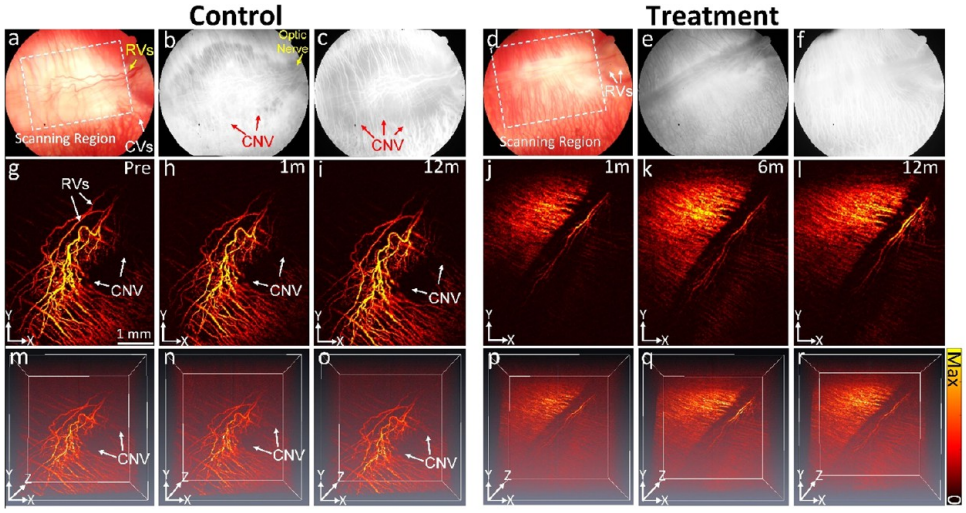

Figure 6. *In vivo* PAM imaging visualization of of rabbits treated with Si NNs. (a) Color fundus photography showing the retinal vessels (RVs), choroidal vessels (CVs), and retinal pigment epithelium (RPE) before treatment. (b) Fluorescein angiography (FA) image highlighting the nerve fiber layer (NFL), RVs, and areas of CNV. (c) Indocyanine green angiography (ICGA) image illustrating CNV and the structure of RVs, CVs, and capillaries. (d–f) Fundus photos and fluorescein angiography taken at 1 month after treatment. PAM images taken before treatment (g), at 1 month (h), and at 12 months (i), corresponding to the scanned area outlined by the white dotted rectangle in (a), providing a high-resolution view of RVs and CNV. (j–l) Two-dimensional PAM images captured at 1-, 6-, and 12-months post-treatment in the Si NN-Bev treated group. (m–o) 3D volumetric PAM reconstructions in control eyes offer a three-dimensional perspective of RV and CNV morphology. (p–r) 3D volumetric PAM images further illustrate the vascular structures over time in Si NN-Bev treated eyes.

of CNV, along with associated retinal layers and choroidal vessels. Following treatment initiation, progressive reduction in CNV dimensions and alterations in lesion margins were observed over time (Figure 4b–f), indicative of treatment response.

Quantitative analysis of mean CNV thickness and mean lesion density (Figure 5) further elucidated treatment response dynamics. At 12 months post-treatment, a substantial reduction in CNV thickness with an average of 83% was observed compared to baseline (CNV thickness = 0.17 ± 0.04 (a.u.) at 12 months post-treatment vs 1.00 ± 0.00 (a.u.) at pretreatment), highlighting initial evidence of therapeutic efficacy (Figure 5a). In contrast, the control group, Bev only group and Si NNs without conjugation with Bev exhibited minimal changes in CNV thickness (2–20%) over the same period (CNV thickness = 0.79 ± 0.04 (a.u.) at 12 months post-treatment vs 1.00 ± 0.00 (a.u.) at pretreatment). Similarly, the CNV density (VD) exhibited a significant reduction following treatment. Post-treatment, the VD decreased by approximately 82% compared to pretreatment levels, whereas the control group showed only a modest 8% reduction in CNV density (Figure 5b). This suggests the substantial therapeutic impact of the treatment on CNV density.

In Vivo Photoacoustic Microscopy (PAM) Imaging

We next conducted PAM imaging to delineate the localization and morphology of CNV. Prior to PAM, we captured the color fundus photography (Figure 6a), FA (Figure 6b), and ICGA (Figure 6c) to determine the scanning area for PAM as well as to visualize the growth of CNV. CNV was clearly visualized on both FA and ICGA. Figure 6g–i illustrates PAM images obtained from the control group before and after treatment along the scanning areas shown in Figure 6a, revealing distinct visualization of CNV lesions alongside retinal vessels (RVs), choroidal vessels (CVs), and capillaries with high contrast. There were no significant differences observed over time in the control group images, indicating minimal changes in CNV characteristics. In contrast, Figure 6j–r depicts PAM images from the treatment group acquired along the scanning areas shown in Figure 6d–f, where major RVs, CVs, and capillaries were prominently visualized with high contrast and high resolution. Notably, a reduction in vessel density was noted post-treatment, suggestive of treatment-induced effects on vasculature and regression of newly formed vessels. Furthermore, Figure 6m–o and p–r exhibit 3D-rendered volumetric PAM images, offering comprehensive visualization of RVs, CVs, capillaries, and CNV at varying depths. Remarkably, diminished CNV signal was evident in the treated group (Figure 6p–r, Supplementary Videos S4–S6), whereas stable CNV visualization was observed in the control group (Figure 6m–o, Supplementary Videos S1–S3), highlighting the efficacy of the Si NNs-Bev treatment in treating CNV, and reducing its detectable presence in PAM imaging. These findings emphasize the utility of PAM imaging in elucidating CNV dynamics and treatment responses, offering valuable insights into therapeutic efficacy and disease progression in CNV-associated retinal pathologies.

In Vivo Biosafety Analysis

We next conducted an *in vivo* biosafety analysis to evaluate the potential toxicity of Si NNs in animals. The subconjunctival Si NNs patch represents a *minimally invasive* delivery route. Facial expression monitoring using the rabbit grimace scale score (RGS) (Supporting Information Figure S8) was employed to quantify potential discomfort. The mean RGS scores remained consistently low (below 4) for all groups throughout the study, indicating no observable signs of significant pain. These quantitative results were further verified by longitudinal initial daily and later weekly slit-lamp examinations showing an absence of acute erythema, edema, or mucopurulent inflammation. The conjunctival insertion site was observed to heal rapidly, with the micropenetrations made by the nanoneedles self-sealing within minutes due to the elasticity of the subconjunctival tissue, leaving no visible scarring or fibrosis

https://doi.org/10.1021/acsbiomaterials.5c01783
ACS Biomater. Sci. Eng. 2026, 12, 1269–1285

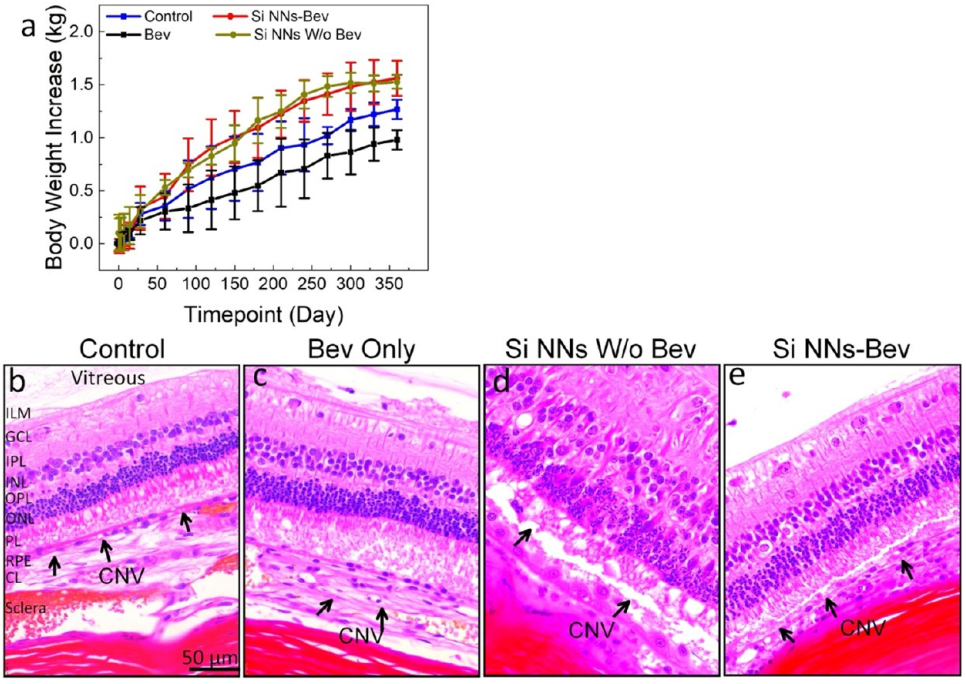

Figure 7. *In vivo* biosafety analysis. (a) Graph depicting the body weight of rabbits over time, comparing groups with and without SiNN-Bev treatment. (b–e) Representative 40× H&E-stained retinal images from control group (b), Bev-only treatment group (c), treatment group with Si NNs without conjugated with Bev (d), and the SiNNs-Bev treatment group with Si NNs-Bev (e). These images clearly identify choroidal neovascularization (CNV) marked by black arrows. The retinal layer architecture is well-defined, including the inner limiting membrane (ILM), ganglion cell layer (GCL), inner plexiform layer (IPL), inner nuclear layer (INL), outer plexiform layer (OPL), outer nuclear layer (ONL), photoreceptor layer (PL), retinal pigment epithelium (RPE), choroid layer (CL), and sclera. Data are presented as Mean ± Standard Deviation (N = 3 per group).

upon long-term follow-up. While qualitative, these findings suggest the procedure is well tolerated in rabbits and likely to be patient-compatible for clinical translation. Next, the body weight of all treated rabbits, including control groups, was monitored initially daily and later weekly before and after treatment for up to 12 months. All animals in each group consistently gained weight over the 12-month study (Figure 7a). Although the Si NNs-treated groups showed a slightly higher mean weight gain compared to the control, statistical analysis confirmed these differences were not significant (p = 0.061). This variation is likely attributed to the inherent biological growth trajectory of the randomized rabbit cohorts and is an incidental statistical noise given the small sample size rather than a treatment-induced effect. No abnormal clinical signs, changes in feeding behavior, or systemic distress were observed in any experimental group throughout the duration of the study.

To assess CNV before and after treatment, animals were euthanized, and H&E staining was performed. The retinal architecture with the formation of CNV was clearly observed on the H&E images (Figure 7b–e). The distinct layers of the retina were also clearly observed on H&E and demonstrated no evidence of toxicity, including in the inner limiting membrane (ILM), ganglion cell layer (GCL), inner plexiform layer (IPL), inner nuclear layer (INL), outer plexiform layer (OPL), outer nuclear layer (ONL), photoreceptor layer (PL), retinal pigment epithelium (RPE), choroid layer (CL), and sclera. Notably, the density of CNV was lower in the group treated with Si NNs-Bev (Figure 7e) compared to the control group (Figure 7b), group treated with Bev only (Figure 7c) and treated with Si NNs without conjugated with Bev (Figure 7d), confirming that SiNN-Bev led to CNV regression.

To evaluate the long-term impact on retinal structure, we quantified the Total Retinal Thickness (TRT) at the 12-month end point. Due to the significant structural remodeling and boundary distortion in the outer retina following Matrigel +VEGF-induced CNV formation, layer-specific segmentation (e.g., INL and ONL) was not feasible with high precision. However, the TRT in the SiNNs-Bev group (123.91 ± 1.38 μm) was statistically indistinguishable from that of the control group (127.59 ± 7.48, p = 0.054). These results indicate that the SiNNs-Bev treatment maintains overall retinal integrity and does not exacerbate the atrophy associated with the disease model.

TUNEL assay results showed no evidence of apoptotic cells in any of the treated groups (Figure 8), further confirming the safety of Si NNs treatment and its potential as a drug delivery system for neurodegenerative disorders. Immunohistochemistry with α-SMA revealed that choroidal vessels formed CNV, which extended through the Matrigel+VEGF injection area and expanded into the subretinal space at the injury sites. Figure 9 indicates that α-SMA immunohistochemistry is effective in identifying new blood vessel formation in subretinal lesions. The density of α-SMA-positive tissue was lower in the SiNN-Bev treated group with Si NNs-Bev (Figure 9a) compared to the Bev-only (Figure 9b), control groups (Figure 9c), or the treatment group with Si NNs without conjugation with Bev (Figure 9d), illustrating that the SiNNs-Bev successfully inhibited the growth of CNV.

https://doi.org/10.1021/acsbiomaterials.5c01783
ACS Biomater. Sci. Eng. 2026, 12, 1269–1285

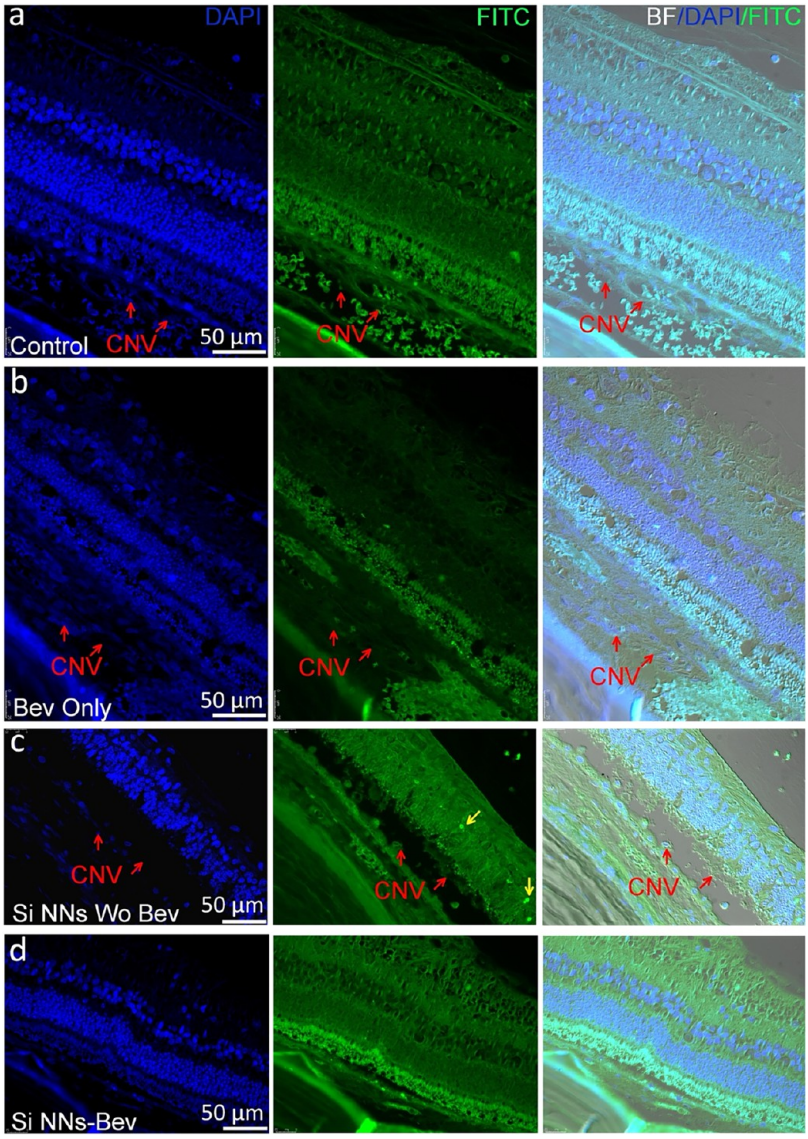

Figure 8. TUNEL assay analysis conducted 12 months post-treatment with Si NNs-Bev. (a) Control group. (b) Treatment group with anti-VEGF bevacizumab (Bev) only. (c) Treatment group with Si NNs without conjugated with Bev. (d) Treatment group with Si NNs conjugated with Bev (Si NNs-Bev). Cell nuclei were stained with DAPI (blue), and apoptotic cells were labeled with FITC (green). No apoptotic cells were observed in any of the groups. Scale bar: 50 μm.

DISCUSSION

The integration of controllably bioresorbable Si NNs on a tear-soluble subconjunctival patch introduces a novel, minimally invasive, and effective long-term route for ocular drug delivery. This innovative method addresses the critical need for alternatives to traditional intravitreal injections, which are often associated with discomfort and potential complications. The Si NNs' ability to embed into the sclera in a minimally invasive manner represents a significant advancement in ocular therapeutics. This approach not only reduces discomfort but also enhances drug delivery precision and efficacy. Furthermore, the risk of endophthalmitis, a rare but vision-threatening complication of intravitreal injections, is significantly mitigated by the nanoneedle design. The SiNN tips (<250 nm) create micropenetrations that are orders of magnitude smaller than a standard 30-gauge needle and, crucially, smaller than common ocular pathogens (0.5−2.0 μm). Because the needles only penetrate the superficial sclera partial thickness and do not breach the vitreous cavity, they do not create a patent tract for bacterial entry. This structural safety, combined with the rapid self-sealing of the nanopores, likely contributed to the absence of any infectious or inflammatory complications throughout the 12-month study period.

The design of Si NNs allows for effective embedding into the ocular sclera without causing significant damage. The controlled gradual degradation of Si NNs over the course of several months is a key feature that distinguishes this approach from conventional bioresorbable composites. This prolonged degradation enables the sustained release of therapeutic agents, maintaining therapeutic drug levels for extended periods and reducing the frequency of required treatments. Such sustained release is particularly advantageous in managing chronic ocular conditions, where long-term drug administration is necessary.

The effectiveness of Si NNs-Bev in treating CNV was demonstrated in a rabbit model of AMD. The Si NNs-Bev treatment group exhibited a strong preliminary trend toward CNV regression with a mean reduction of 82% compared to

https://doi.org/10.1021/acsbiomaterials.5c01783
ACS Biomater. Sci. Eng. 2026, 12, 1269−1285

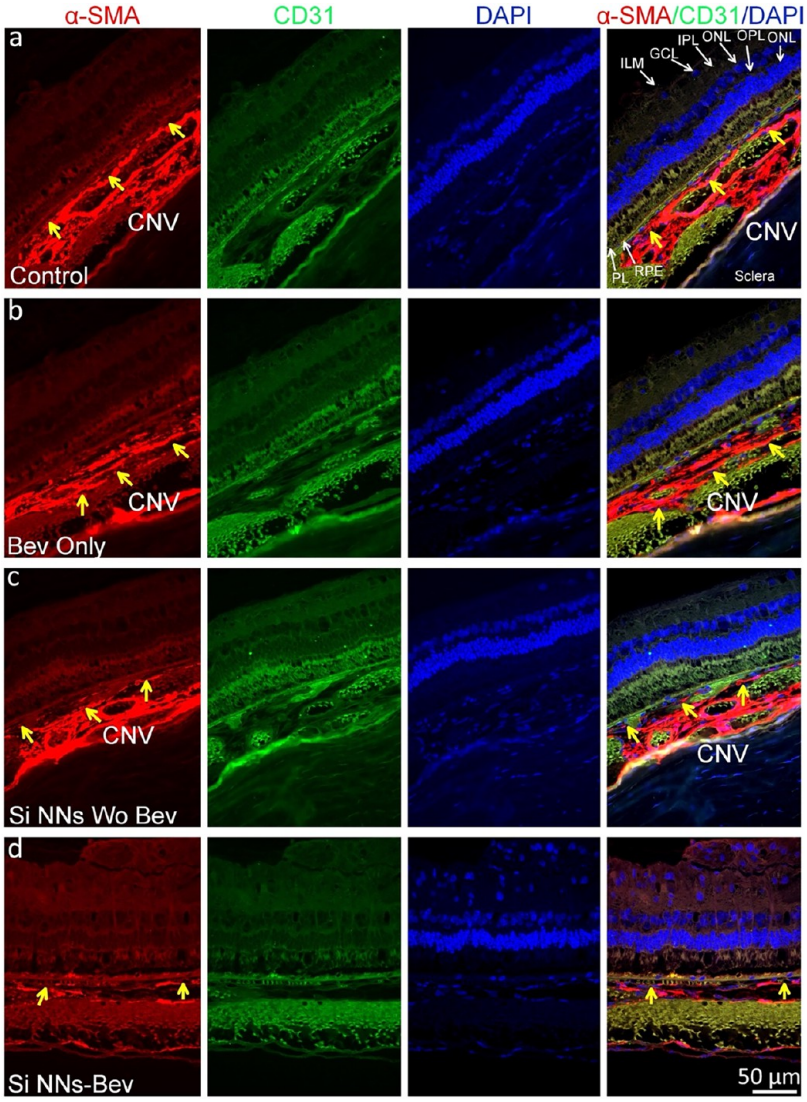

Figure 9. Immunofluorescent imaging of choroidal neovascularization (CNV) following treatment with Si NNs. Fluorescence images of the retinal tissue stained with vascular markers: α-SMA (red) and CD31 (green), while cell nuclei are stained with DAPI (blue). The panels display results from the control group (a), the Bev-only treatment group (b), the treatment group with Si NNs without conjugation with Bev (c), and the Si NNs-Bev treatment group (d). Yellow arrows indicate the locations of vascular walls labeled with α-SMA.

the control group by 5 months that was sustained for up to 1 year. While not statistically powered to provide a definitive conclusion, this significant magnitude of reduction highlights the therapeutic potential of Si NNs-Bev in managing CNV. The minimal recurrence of CNV observed up to 12 months post-treatment suggests the long-term potential of this approach. A major limitation of this study is the small sample size (N = 3 per *in vivo* group). Although this pilot cohort demonstrated the feasibility of the Si NNs−Bev patch and revealed encouraging therapeutic trends, the limited sample size substantially restricts the statistical power of the quantitative imaging analyses (FA and OCT) and limits the generalizability of the findings. Likewise, interpretation of the safety profile remains preliminary and is primarily focused on long-term biocompatibility at the 12-month end point. In addition, early stage molecular markers of inflammation (e.g., cytokine profiling), oxidative stress, and detailed histological evaluations of immune activation or fibrosis at the scleral interface during the acute phase were not assessed. While the long-term results are encouraging, a broader safety panel is essential to fully characterize the tissue response before clinical translation. Future studies will incorporate longitudinal histology at multiple time points (e.g., day 1, 7, and 30) along with quantitative biochemical assays to provide a more comprehensive safety assessment. Accordingly, these results should be regarded as proof of concept and strongly support the need for future studies with adequately powered, larger cohorts to establish statistically robust safety, efficacy, and broader applicability.

The Si NNs-Bev platform provides year-long suppression of CNV by maintaining bevacizumab in a structurally intact and biologically active state throughout the degradation of the silicon matrix. Bevacizumab is covalently immobilized via TESPSA salinization through accessible lysine residues, forming stable amide bonds that preserve tertiary antibody structure. Prior analyses using ELISA, SEC-HPLC, and SDS-PAGE[12] confirmed that TESPSA-mediated conjugation does not denature IgG antibodies and that the released antibodies retain full VEGF-A binding capacity. In our system, bevacizumab release is governed primarily by the gradual

https://doi.org/10.1021/acsbiomaterials.5c01783
ACS Biomater. Sci. Eng. 2026, 12, 1269−1285

dissolution of the silicon nanoneedles (3.5−16.6 nm/day), resulting in a slow and continuous liberation of intact antibody rather than rapid linker hydrolysis. This sustained release maintains long-term VEGFR2 inhibition, reducing endothelial proliferation, vascular leakage, and promoting progressive CNV remodeling over the course of 12 months. While direct PK data were not collected in the present study, the robust biological response supports the maintenance of therapeutically effective local anti-VEGF concentrations.

We acknowledge that while FA, OCT, and PAM imaging convincingly show structural and functional improvement, they remain indirect measures of drug activity. The current mechanistic explanation of CNV suppression is largely descriptive. Future studies will incorporate direct biological validation, including quantification of VEGF expression levels in treated versus control tissue, markers of endothelial proliferation (e.g., CD31, Ki67), and assessments of hypoxia or long-term tissue remodeling to provide an explanatory molecular framework for the observed regression.

The silicon nanoneedles penetrate only ∼20−30 μm into the sclera with tip diameters under 250 nm, creating microindentations that promptly self-seal due to the elasticity of the conjunctival and Tenon's tissues. Combined with the absence of a transscleral fluid conduit, the risk of infection or endophthalmitis is substantially lower than with intravitreal injections. No inflammatory response, infection, or tissue disruption was observed at any time point over 12 months. Retinal thickness measurements showed no structural toxicity. Future studies will include early inflammatory markers, cytokine profiling, and fibrosis assessment to fully characterize acute and chronic tissue response. While our morphological analysis and TUNEL staining (Figure 7) demonstrate long-term structural biocompatibility, further functional assessment using electroretinography (ERG) in future studies can be used to definitively rule out subtle physiological changes in retinal function prior to clinical application.

In vitro SEM and mass-loss analyses confirm uniform degradation of Si NNs over time, consistent with previously reported hydrolytic dissolution rates. *In vivo*, dissolution of the PVA backing occurs within 1 min, as shown in our Supplementary Video S7, allowing firm embedding of the nanoneedles into the sclera. While *in vivo* nanoneedle degradation is challenging to quantify directly, the absence of CNV recurrence, unlike the leakage relapse observed in the bevacizumab injection group, suggests prolonged release beyond 4 months and possibly up to the full 12-month study end point. Based on the nanoneedle geometry (2 μm base diameter) and measured degradation rates (3.5−16.6 nm/day), the platform is theoretically designed to sustain drug release for approximately one year. The observed level in CNV regression after 4 months indicates a functional stabilization of the retinal architecture rather than a stage in drug concentration. Furthermore, this slow-degradable mechanism facilitates a near zero-order release, which maintains Bev levels within the therapeutic window for a significantly longer duration than single injections. As the nanoneedles gradually degrade, the release rate decreases accordingly, providing a controlled and safe transition as the therapeutic payload is gradually released. The release rate is expected to diminish gradually as the silicon thickness decreases, potentially enabling extended therapeutic exposure while avoiding supra-therapeutic dosing.

Wafer-scale fabrication enables batch-consistent nanoneedle geometry, and the platform is compatible with standard semiconductor manufacturing. Mechanical robustness testing from prior work demonstrates that nanoneedles withstand manual handling and ocular placement. Sterilization with UV or ethanol does not affect antibody function. Unlike subretinal injections which require vitrectomy surgery, the Si NNs patch offers a minimally invasive approach capable of bypassing ocular barriers while delivering long-term therapy with a single application. Future clinical translation will require larger-scale preclinical studies, PK mapping, multidose comparison with currently approved anti-VEGF therapeutics, and human-factors evaluation for reproducible patch placement.

We acknowledge that a comprehensive elucidation of the local and sustained antiangiogenic mechanism mediated by the Si NNs platform remains necessary. The current findings are primarily descriptive, focusing on the structural and functional outcomes of the treatment. Future studies will incorporate targeted *in vitro* assays, including VEGF-stimulated endothelial cell proliferation and tube formation assays, to directly quantify inhibition of VEGF-driven cellular processes. In parallel, *in vivo* investigations will correlate Si NN degradation and bevacizumab release kinetics with longitudinal changes in VEGF expression and vascular remodeling markers such as Ki67 and CD31 and fibrosis (e.g., α-SMA), enabling a more precise characterization of the sustained antiangiogenic mechanism.

The comparison between a single application of the Si NNs−Bev patch and a single acute bevacizumab injection was intentionally designed to assess the sustained-release capability of the Si NNs platform relative to an equivalent acute drug dose. However, we recognize that this bevacizumab-only control does not reflect the current clinical standard of care, which relies on repeated, scheduled intravitreal injections of both FDA-approved anti-VEGF agents such as ranibizumab or aflibercept along with bevacizumab. Consequently, while our findings demonstrate the superiority of sustained release over a single acute dose, they do not yet establish therapeutic equivalence or superiority relative to a clinically relevant, multidose regimen.

Therefore, although the data support the sustained therapeutic benefit of the Si NNs platform, any assertion that this technology could reduce or replace repeated intravitreal injections remains speculative and must be validated in future chronic studies directly comparing the patch with standard multidose injection protocols. Such studies will constitute a critical next step in translational development. Nonetheless, the minimally invasive application, extended drug-release profile, and marked reduction in CNV burden underscore the potential of the Si NNs patch as a clinically relevant and patient-friendly approach for long-acting ocular drug delivery, particularly given its ease of application without the need for intravitreal procedures.

The use of advanced imaging techniques, such as optical coherence tomography (OCT) and photoacoustic microscopy (PAM), allowed for precise monitoring of CNV progression and treatment outcomes. These imaging modalities provided detailed insights into the CNV margins and location, confirming the stability and regression of CNV in Si NN-Bev treated eyes. The ability to monitor treatment efficacy in real-time is crucial for optimizing therapeutic strategies and ensuring successful outcomes. Longitudinal 2D OCT imaging was used to assess CNV regression, offering detailed insights into treatment response and retinal structural changes. The

https://doi.org/10.1021/acsbiomaterials.5c01783
ACS Biomater. Sci. Eng. 2026, 12, 1269−1285

gradual reduction in CNV size, along with alterations in lesion morphology, indicates therapeutic effectiveness. This highlights the value of OCT as a noninvasive tool for tracking disease progression and treatment outcomes. Furthermore, the structural changes observed in the retina following CNV induction emphasize the complex pathological mechanisms involved in CNV-related retinal diseases.

Additionally, minimal side effects on ocular tissues or systemically were observed following Si NNs-Bev treatment, indicating the biocompatibility and safety of this delivery system. Histological analysis revealed no significant inflammation or adverse tissue reactions, which is important for possible future clinical translation of this technology. The favorable safety profile of Si NNs supports their potential evaluation in a wide range of ocular applications, offering a less invasive, long-term, and more tolerable alternative to existing treatments. Yet, the versatility of Si NNs extends beyond the treatment of CNV. The ability to load Si NNs with various ocular drugs opens up new possibilities for treating a broad range of chronic ocular diseases, including glaucoma, diabetes, dry eyes, uveitis, eye cancers, and allergies. This flexibility makes Si NNs a promising platform technology for delivering different therapeutic agents, tailored to specific ocular conditions. Future research should explore the application of Si NNs in these areas, aiming to enhance treatment efficacy and outcomes.

While the current study successfully validated the sustained therapeutic efficacy of the SiNN-Bevacizumab patch through functional imaging and histological analyses over 12 months, a key limitation is the absence of direct, mechanistic evidence confirming the proposed drug distribution pathway. The sustained suppression of CNV activity (Figure 4 and Figure 5) is highly consistent with the working hypothesis that the SiNNs enable transscleral delivery, bypassing the inner limiting membrane (ILM) barrier and maintaining a localized diffusion gradient toward the choroid to suppress the CNV. However, the manuscript currently lacks direct proof of this mechanism. Specifically, we did not include direct evidence of drug penetration patterns, such as tracking with fluorescently labeled bevacizumab, quantitative mass spectrometry of drug concentrations across the retina and choroid, or immunohistochemistry to visualize VEGF suppression gradients. We recognize the critical nature of these experiments and are actively planning dedicated follow-up studies to definitively visualize the localized drug distribution and quantify its concentration profile across the posterior pole tissues. With these limitations acknowledged, the current functional results provide compelling initial proof-of-concept for the SiNN patch as a novel platform for highly localized, long-term ocular drug delivery. The gradual hydrolysis of Si into orthosilicic acid ($Si(OH)_4$) proceeds via physiologic aqueous reactions and yields biocompatible degradation products that are naturally cleared through tear fluid and uveal vasculature, consistent with prior reports demonstrating no inflammation or immune activation in ocular tissues.[31,33] Although pharmacokinetic quantification was beyond the scope of this study, future work will correlate Si NN degradation and Bevacizumab release kinetics with longitudinal VEGF expression and vascular remodeling markers to elucidate the mechanism of sustained antiangiogenic effect.

Although continuous *in vivo* visualization of silicon nanoneedle degradation over the entire study period was not performed, the long-term therapeutic efficacy observed over 12 months, together with the absence of tissue damage, inflammation, or fibrosis in histological analyses, supports gradual and controlled biodegradation of the Si NNs under physiological conditions. Consistent with prior *in vitro* degradation studies of the same Si NNs platform,[5] these findings indicate that the nanoneedles persist for extended durations and degrade slowly rather than undergoing rapid dissolution or mechanical failure *in vivo*.

In the present study, sustained therapeutic efficacy against CNV is supported primarily by long-term *in vivo* outcomes rather than by standalone *in vitro* release measurements. The Si NNs−Bev platform differs from conventional reservoir-based delivery systems because Bevacizumab is immobilized on the nanoneedle surface and drug presentation is governed mainly by gradual, material-driven biodegradation of the silicon nanoneedles rather than diffusion-controlled release. Accordingly, previously reported *in vitro* release studies using the same Si NNs configuration are cited as mechanistic context supporting prolonged drug presentation, while future work will include quantitative *in vitro* release profiling and pharmacokinetic measurements to further correlate release kinetics with ocular drug levels and therapeutic outcomes.

CONCLUSIONS

The integration of controllably bioresorbable Si NNs with tear-soluble subconjunctival patches represents an innovative approach to ocular drug delivery. This method offers significant advantages in terms of minimal invasiveness, prolonged drug release, and safety, addressing the limitations of traditional ocular therapies. The successful application of Si NNs-Bev in regressing CNV by 82% that persists for 1 year in an AMD model highlights the therapeutic potential of this technology. With further research and development, Si NNs could revolutionize the treatment of a wide range of chronic ocular diseases. In addition, this study demonstrates the utility of multimodal imaging in longitudinally evaluating CNV regression and structural alterations following treatment. The progressive reduction in CNV dimensions and associated changes in retinal architecture underscore the efficacy of therapeutic interventions in treating CNV. These findings emphasize the importance of regular imaging monitoring in optimizing treatment strategies and improving outcomes in CNV-associated retinal diseases.

MATERIALS AND METHODS

Fabrication of Si NNs on Si Wafer

The fabrication of Si NNs began with conventional cleaning process for a bulk Si wafer (525 μm thick; 0 to 100 Ω·cm) using sulfuric peroxide mixture (SPM) and a diluted HF solution. The next step involved photolithographic patterning and deep reactive ion etching (DRIE) to initially define micropillar arrays, utilizing specific parameters such as a radiofrequency (RF) plasma power of 450 W and a platen power of 11 W, along with sulfur hexafluoride (SF_6) gas at a flow rate of 85 sccm (standard cubic centimeters per minute). A thin $(C_xF_y)_n$ polymer layer was passivated to the surface of the Si micropillars using octafluorocyclobutane (C_4F_8) gas at a flow rate of 130 sccm and a RF plasma power of 800 W. The bottom of the Si micropillars were intentionally left unpassivated, followed by an anisotropic dry etching process to create undercuts using sulfur hexafluoride (SF_6) gas at a flow rate of 85 sccm, with RF plasma power and platen power set at 450 and 14 W, respectively. The specimen was then treated with oxygen (O_2) plasma and SPM to remove residues such as the photoresist and the passivation polymer layer. To shrink the size of the Si micropillars from microscale to

https://doi.org/10.1021/acsbiomaterials.5c01783
ACS Biomater. Sci. Eng. 2026, 12, 1269−1285

nanoscale, the Si pillars were immersed in phosphate-buffered saline (PBS; pH 7.4) at 67 °C and in a 15 wt % potassium hydroxide (KOH) solution at 25 °C for 10 min. A MACE process followed, immersing the Si NNs in a mixture (20 mM $AgNO_3$ in 49% hydrogen fluoride) to form a nanoporous surface, and then immediately removing Ag residues with an Ag etchant solution for 1 min. Finally, a thin film of Al_2O_3 was deposited by ALD with each cycle designed to deposit a 1 Å thickness for a total of 30 cycles.

Integration of Biodegradable Patch with Si NNs

The as-prepared Si NNs on a Si wafer was coated with a 200 μm thick layer of PMMA film by spin-casting, and then they were thermally cured in a vacuum chamber at 80 °C for 2 h. Surface tension effects caused an air gap of about 5 μm between the Si wafer and PMMA layer during this process. The PMMA layer was then mechanically peeled off with a Mark-10 equipment (Willrich Precision Instruments) at a steady rate of 50 mm/min. The bottom root of Si NNs was exposed to one side of the PMMA film that had 500 μL of the PVA solution (molecular weight = 31,000; 2 wt %) drop-cast onto it. The PVA solution was then allowed to cure in a vacuum chamber at 60 °C for an hour. This step was carried out three times under the same conditions to obtain a PVA film with a thickness of 40 μm. The resulting structure, which consisted of a double-layered PMMA−PVA film, was subsequently immerged in acetone at 70 °C for 4 h to selectively remove the PMMA layer. Before each use, the biodegradable patch with implanted Si NNs was sterilized by soaking it in an anhydrous ethanol bath for 5 min and then exposing it to UV light with a wavelength of 254 nm for 5 min.

Animal Preparation

All animal experiments were conducted in compliance with the ARVO (The Association for Research in Vision and Ophthalmology) guidelines for the Use of Animals in Ophthalmic and Vision Research. The study protocol was approved by the Institutional Animal Care & Use Committee (IACUC) at the University of Michigan (Protocol PRO00010388, PI: Paulus). Adult New Zealand White (NZW) rabbits of both genders, weighing between 2.15 and 2.42 kg and aged 3 to 6 months, were used in this study. Animals were randomly assigned to treatment groups without stratification by gender. Anesthesia was induced with an intramuscular injection of ketamine (40 mg/kg) and xylazine (5 mg/kg), with one-third of the ketamine dose administered additionally at 45 min intervals during the experiment to maintain anesthesia. Pupil dilation was achieved using phenylephrine hydrochloride 2.5% and tropicamide 1% ophthalmic solution. Topical tetracaine ophthalmic drops were applied to the rabbit's eyes for additional local anesthesia. Vital signs, including mucous membrane color, heart rate, respiratory rate, and body temperature, were monitored and recorded every 15 min during anesthesia and recovery. Heart rate and respiratory rate were measured using a SpO2 Digital Pulse Oximeter (V8400D, MWI Animal Health, Boise, ID). Body temperature was maintained with a water circulation blanket (TP-700, Stryker Corporation, Kalamazoo, MI). Additionally, balanced salt solution was applied to the eyes every minute to prevent corneal dehydration (Altaire Pharmaceuticals, Inc., Aquebogue, NY).

AMD Clinically Relevant CNV Disease Model

A choroidal neovascularization (CNV) model was created in 15 rabbits using a subretinal injection procedure as previously described.[34,35] Briefly, Matrigel basement membrane matrix (Corning, NY, USA) combined with human vascular endothelial growth factor (VEGF-165, Shenandoah Biotechnology, Warwick, USA) was employed to induce CNV. Prior to the subretinal administration, a stock solution of VEGF-165 was prepared at a final concentration of 100 μg/mL in 1% bovine serum albumin. Subsequently, 20 μL of Matrigel was mixed with 750 ng of VEGF. This mixture was injected into the subretinal space of the retina of the anesthetized rabbits using a 30-gauge needle (Hamilton, NV, USA). The needle direction and target location were monitored using a microscope (Amscope, USA) during the injection. Once the needle reached the subretinal space, the solution was administered into the subretinal area. The needle was then carefully withdrawn to avoid contact with the lens to avoid inducing a cataract. The injection blebs were confirmed with color fundus photography and optical coherence tomography (OCT). CNV progression was monitored using multimodal imaging, including color fundus photography, fluorescein angiography (FA), indocyanine green angiography (ICGA), OCT, and photoacoustic microscopy (PAM) imaging.

CNV Treatment Procedure

To treat CNV, all animals received subconjunctival treatments. Three days after CNV induction via subretinal injection of Matrigel and VEGF, the rabbits were administered Si NNs treatment. The rabbit models were divided into four treatment groups: a control group (treated with vehicles or PBS, $N = 3$), a group treated with intravitreal Bev only ($N = 3$), a group treated with Si NNs without Bev ($N = 3$), and a group treated with Si NNs-Bev ($N = 3$). Before treatment, a localized quadrant peritomy was performed using Westcott scissors and then Tenon's was dissected carefully using 0.12 forceps and Westcott scissors (Supporting Information Figure S8). An artificial tear gel (Alcon, USA) was applied, followed by the insertion of Si NNs patches. To facilitate the dissolution of Si NNs and prevent corneal dehydration, additional artificial tear drops (Alcon, USA) were applied regularly. The Si NNs patches completely dissolved within 1 min postapplication, as demonstrated by direct visual evidence in Supporting Information Videos 7 (*in vivo*) and 8 (*in vitro*, porcine eye model). The progression of CNV was monitored before and after Si NNs treatment for up to 12 months using multimodal imaging.

Ophthalmoscopic Examination

Comprehensive ophthalmoscopic examinations were conducted on all rabbits at 3, 5, 7, 14, 21, and 28 days followed by monthly up to 12 months post-treatment. A slit lamp biomicroscope (Zeiss SL130 slit lamp, Carl Zeiss Meditec, Germany) was used to inspect for signs of eye inflammation, infection, and cataract formation, as well as erythema or edema at the injection site.

Fundus Photography and Fluorescein Angiography Imaging of CNV

Retinal blood vessel and CNV imaging before and after Si NNs-Bev treatment was performed using 50° color fundus photography (Topcon 50EX, Topcon Corporation, Tokyo, Japan). These images were taken from various angles and positions within the eye to observe the effects of Si NNs-Bev on specific regions such as optic nerve, inferior retina, superior retina, and the temporal and nasal medullary rays. Fundus fluorescein angiography (FA) was conducted alongside fundus photography to evaluate the CNV and retinal vasculature. A 0.2 mL solution of 10% sodium fluorescein (Akorn, Lake Forest, IL, USA) was injected into the marginal ear vein. Images were taken in quick succession immediately following the injection and then at 1 min intervals for a total duration of 15 min.

Multimodal OCT and PAM Imaging

In this study, we performed OCT and PAM imaging on the treated animals using a custom-built multimodality photoacoustic (PA) and OCT imaging system[36−44] to longitudinally evaluate CNV dynamics post-treatment. PA imaging is a novel noninvasive and nonionizing imaging technique that uses laser pulse generated thermal expansion of tissue to create acoustic waves which can be detected by a transducer.[45−47] PA allows imaging of deeper retinal and choroidal vasculature that may be otherwise missed by OCT imaging. OCT imaging allows clear visualization of the individual layers of the eye and surface level CNV progression; however, it lacks the ability to see deeper CNV with high resolution, especially in pigmented eyes.[48] Fluorescein angiography can easily pick up signs of CNV leakage as seen in diseases such as wet AMD. By combining data from these imaging modalities, we are able to clearly visualize the choroidal and retinal vasculature and CNV alleviation from treatment.[49] The OCT and PAM imaging were performed at various time points over a 12-month period following therapeutic intervention. OCT images were analyzed to assess CNV dimensions, retinal architecture, and

https://doi.org/10.1021/acsbiomaterials.5c01783
ACS Biomater. Sci. Eng. 2026, 12, 1269−1285

treatment response. Quantitative measurements of CNV thickness and lesion density were obtained using standardized techniques. For imaging, anesthetized rabbits were positioned on separate stages to minimize movement artifacts. To maintain coupling between the ultrasound transducer and the conjunctiva, balanced salt solution (BSS) was applied to the cornea regularly every minute. PAM images were captured at an excitation wavelength of 578 nm to visualize the choroidal and retinal vascular networks. The imaged area was approximately 4.5 × 4.5 mm^2 with a resolution of 256 × 256 pixels. Three-dimensional PAM images were rendered using Amira 6.0 (Visualization Sciences Group).

Grimace Scale Evaluation

To evaluate animal comfort following treatment with a subconjunctival patch, a grimace scale assessment was conducted.[50] Digital images of the animals' faces were captured before and after treatment, and these images were analyzed for potential signs of discomfort. Key facial features, including the shape of the nose (particularly the V-shape), orbital tightening, cheek flattening, ear shape and orientation, as well as whisker shape and position, were closely examined. The grimace scale, a validated, reliable, and noninvasive method for assessing pain and discomfort in rabbits, quantifies specific facial expressions that are indicative of distress. This analysis is essential for assessing the treatment's comfort and ensuring the animals' well-being.

In Vivo Biosafety Evaluation

To evaluate the potential side effects to the animal, we performed a comprehensive *in vivo* biosafety analysis including monitoring the animals' body weight, standard hematoxylin and eosin (H&E), TUNEL assay, and immunohistochemistry. Each animal was weighed before and after treatment and followed for 12 months. The body weight was analyzed and plotted using Origin software (Origin 9.0, OriginLab, MA, USA). To perform H&E and TUNEL staining, the animals were euthanized at 12 months post-treatment. The eyeballs were harvested and fixed with Davidson's fixative solution (Fisher Scientific, MD, USA) for 24 h. Then, the samples were transferred to 50% alcohol for 8 h and 70% alcohol for an additional 24 h before sectioning. To section the sample, the tissues were cut into two-halves at the center of the optic nerve and embedded in parraffin. Afterward, the tissues were sectioned with a thickness of 6−8 μm using a microtome followed by staining with H&E. The slides were then analyzed using DM6000 Leica Microscope (DM6000, Leica Biosystems, Nussloch, Germany). Digital photographs were obtained using a DF450C camera integrated in the microscope.

In Vivo Toxicity Evaluation

TUNEL assay analysis was performed to evaluate the potential toxicity of Si NNs on retinal tissue using the TUNEL *in situ* Cell Death Detection Kit (Sigma-Aldrich, USA). This assay detects apoptotic cells by labeling DNA strand breaks with fluorescently tagged nucleotides. Retinal tissue sections were first fixed and permeabilized to allow reagent penetration. Samples were then incubated with a reaction mixture containing terminal deoxynucleotidyl transferase (TdT) enzyme, which attaches labeled nucleotides to the 3′−OH ends of fragmented DNA. Following incubation, unincorporated nucleotides were washed away. Under a fluorescence microscope, apoptotic cells were visualized as bright fluorescent spots, indicating DNA fragmentation and confirming cell apoptosis.

Immunohistochemistry Analysis

Immunofluorescence staining was performed to confirm the presence of choroidal neovascularization (RNV). Paraffin-embedded slides were initially fixed in 4% paraformaldehyde (PFA) for 15 min at room temperature, followed by permeabilization with 1% saponin in PBS for 30 min. The slides were then incubated overnight at 4 °C in a blocking solution containing 1% bovine serum albumin (BSA) and 10% goat serum in PBS. Primary antibodies, CD31 (P8590, Sigma-Aldrich, USA) and mouse antialpha smooth muscle actin (αSMA) (A2547, Sigma-Aldrich, MA, USA), were applied at a 1:1000 dilution in blocking buffer and incubated overnight at 4 °C. After washing with 0.1 M phosphate buffer (PB), Alexa Fluor 488-conjugated goat antirabbit IgG (A11008, Thermo Fisher, MD, USA) was applied at a 1:500 dilutions in blocking buffer and incubated for 2 h at room temperature in the dark. The samples were then washed again with 0.1 M PB and mounted with ProLong Gold Antifade Mountant with DAPI (P36941, Invitrogen, MA, USA) to stain the nuclei. The slides were examined using a DM6000 microscope (Leica Microsystems Inc., IL, USA), and images were captured with a BFX365 camera.

Image Segmentation

To assess the efficiency of the treatment effect between different treatment groups, we measured fluorescent intensity (FLI) and vessel density (VD) at various time points. Initially, we segmented the choroidal neovascularization (CNV) area using a MATLAB (MathWorks, CA, USA) image segmentation algorithm as shown in Figure S4. We enhanced the contrast of the fluorescent images using an adaptive histogram equalization function. Following this, the boundary of the fluorescent leakage area was identified using an edge detection function. FLI was determined by calculating the mean value of each pixel within the extracted area. For each time point, FLI was normalized, with the pretreatment time point set to a value of 1, and relative values were calculated for each subsequent time point post-treatment. VD was measured by counting the pixels along the extracted fluorescent leakage area, and it was normalized by comparing the VD before treatment to the VD after treatment.

α-SMA Immunofluorescence Quantification. Fibrosis within the CNV lesions was assessed by quantifying the α-smooth muscle actin (α-SMA) positive signal. The acquired IHC images were processed using ImageJ software (National Institutes of Health, USA). Briefly, these images were converted to 8-bit grayscale, and a consistent threshold was applied across all experimental groups to exclude nonspecific background signal. The α-SMA positive area was then measured and expressed as a percentage of the total image area (%Area). This standardized thresholding approach was utilized to provide an objective, quantitative comparison of myofibroblast activation between the SiNNs-Bev treated and control groups.

Statistics Evaluation

Statistical analysis was conducted using a one-way ANOVA followed by Tukey's post hoc test to assess the significance between treatment groups. This analysis was carried out using Origin software (OriginLab Corporation, MA, USA). Data were presented as mean values ± standard deviation, and differences between treatment groups were deemed statistically significant when $p < 0.05$.

■ ASSOCIATED CONTENT

Data Availability Statement

The data that support the plots and other findings of this study are available from the corresponding authors upon reasonable request.

Supporting Information

The Supporting Information is available free of charge at https://pubs.acs.org/doi/10.1021/acsbiomaterials.5c01783.

Silicon Nanoneedle Patches for Painless, Sustained Treatment of Macular Degeneration.docx Additional color photography and fluorescein angiography images of the Si NNs-Bev treated group. Color photography and fluorescein angiography images of CNV treated with Si NNs alone, without conjugation with Bev. Color fundus photography and fluorescein angiography (FA) images of CNV treated with Bev alone. Image segmentation processing. Image segmentation depicting extracted regions of interest (ROI) for leakage areas at various time points before and after treatment. Grimace scale analysis of the rabbit pre and post treatment with a sclera-embedded silicon nanoneedles (Si NNs) patch.

https://doi.org/10.1021/acsbiomaterials.5c01783
ACS Biomater. Sci. Eng. 2026, 12, 1269−1285

Procedure for CNV treatment using a sclera-embedded silicon nanoneedles (Si NNs) patch (PDF)

Demonstrates the 3D volumetric rendering of CNV pre-treatment obtained from control group (Movie S1) (MPG)

3D volumetric rendering of choroidal neovascularization (CNV) at 1-month post-treatment, visualized from the control group (Movie S2) (MPG)

3D volumetric rendering of CNV at 12 months post-treatment from the control group (Movie S3) (MPG)

3D volumetric rendering of CNV at 1-month post-treatment, obtained from the Si NNs-Bev-treated group (Movie S4) (MPG)

3D volumetric rendering of CNV at 6 months post-treatment from the Si NNs-Bev-treated group (Movie S5) (MPG)

3D volumetric rendering of CNV at 12 months post-treatment, obtained from the Si NNs-Bev-treated group. (Movie S6) (MPG)

CNV treatment using a sclera-embedded silicon nanoneedles (Si NNs) patch in living rabbits (Movie S7) (MP4)

Time lapse of Si NNs patch dissolution *in vitro* (Movie S8) (MP4)

AUTHOR INFORMATION

Corresponding Authors

Yannis M. Paulus − *Department of Ophthalmology, Wilmer Eye Institute and Department of Biomedical Engineering, Johns Hopkins University, Baltimore, Maryland 21287, United States; Department of Ophthalmology and Visual Sciences and Department of Biomedical Engineering, University of Michigan, Ann Arbor, Michigan 48105, United States;* orcid.org/0000-0002-0615-628X; Email: ypaulus1@jh.edu

Chi Hwan Lee − *Weldon School of Biomedical Engineering, Purdue University, West Lafayette, Indiana 47907, United States; School of Mechanical Engineering, School of Materials Engineering, Elmore School of Electrical and Computer Engineering, and Birck Nanotechnology Center, Purdue University, West Lafayette, Indiana 47907, United States;* orcid.org/0000-0002-4868-7054; Email: lee2270@purdue.edu

Authors

Van Phuc Nguyen − *Department of Ophthalmology, Wilmer Eye Institute, Johns Hopkins University, Baltimore, Maryland 21287, United States; Department of Ophthalmology and Visual Sciences, University of Michigan, Ann Arbor, Michigan 48105, United States;* orcid.org/0000-0001-7466-1483

Jinheon Jeong − *Weldon School of Biomedical Engineering, Purdue University, West Lafayette, Indiana 47907, United States*

Josh Zhe − *Department of Ophthalmology and Visual Sciences, University of Michigan, Ann Arbor, Michigan 48105, United States*

Mi Zheng − *Department of Ophthalmology, Wilmer Eye Institute, Johns Hopkins University, Baltimore, Maryland 21287, United States; Department of Ophthalmology and Visual Sciences, University of Michigan, Ann Arbor, Michigan 48105, United States; Ophthalmology Department, Fujian Provincial Hospital, Fuzhou, Fujian 350001, China*

Junsang Lee − *Weldon School of Biomedical Engineering, Purdue University, West Lafayette, Indiana 47907, United States*

Khoi Tran − *Department of Ophthalmology and Visual Sciences, University of Michigan, Ann Arbor, Michigan 48105, United States*

Zhuying Wei − *Center for Advanced Models for Translational Sciences and Therapeutics, University of Michigan, Ann Arbor, Michigan 48109, United States*

Complete contact information is available at: https://pubs.acs.org/10.1021/acsbiomaterials.5c01783

Author Contributions

V.P.N., J.J., J.L., C.H.L., and Y.M.P. contributed to various aspects of the project, including the concept and design of Si NNs fabrication, as well as interpreting the experimental results. V.P.N. conducted and analyzed the *in vitro* and *in vivo* experiments. J.J., J.L., and C.H.L. were involved in the fabrication and characterization of the soluble Si NNs subconjunctival patch. J.Z. and K.T. assisted with graphical design, while M.Z. and Z.W. provided support with TUNEL and immunofluorescence staining. K.T., J.Z. and M.Z. also contributed to the evaluation of OCT data. The manuscript was written by V.P.N., J.Z., C.H.L., and Y.M.P., with all authors participating in its writing, critical review, and revision.

Funding

This project was supported by grants from the National Eye Institute (Y.M.P.: 1R01EY033000, 1R01EY034325, 1K08EY027458; C.H.L.: R01EY033000), as well as the Fight for Sight-International Retinal Research Foundation (Y.M.P.: FFSGIA16002), the Alcon Research Institute Young Investigator Grant (Y.M.P.), and unrestricted departmental funding from Research to Prevent Blindness. Additional support came from the Dr. Jonas Friedenwald Professorship in Ophthalmology (Y.M.P.) and the Wilmer Eye Institute Department of Ophthalmology. This research also made use of the Core Center for Vision Research, funded by the National Eye Institute (P30 EY007003). C.H.L. acknowledges the support from the Ministry of Trade, Industry and Energy (MOTIE) and Korea Institute for Advancement of Technology (KIAT) through the "International Cooperative R&D program (P0028319)" particularly for developing transfer printing methods and biodegradable devices.

Notes

The authors declare the following competing financial interest(s): YMP and CHL are co-inventors on a Purdue University and University of Michigan patent application on this technology. All of the other authors declare no competing financial interests.

ACKNOWLEDGMENTS

Special thanks to Drs. Yuqing Chen, Dongshan Yang, and the University of Michigan CAMTraST for generously donating rabbits for this research.

REFERENCES

(1) Zhang, K.; Zhang, L.; Weinreb, R. N. Ophthalmic drug discovery: novel targets and mechanisms for retinal diseases and glaucoma. *Nat. Rev. Drug Discovery* **2012**, *11*, 541−559.

(2) Clark, A. F.; Yorio, T. Ophthalmic drug discovery. *Nat. Rev. Drug Discovery* **2003**, *2*, 448−459.

(3) Ganugula, R.; Arora, M.; Lepiz, M. A.; et al. Systemic anti-inflammatory therapy aided by double-headed nanoparticles in a canine model of acute intraocular inflammation. *Sci. Adv.* **2020**, *6*, No. eabb7878.
(4) Ghosh, J. G.; Nguyen, A. A.; Bigelow, C. E.; et al. Long-acting protein drugs for the treatment of ocular diseases. *Nat. Commun.* **2017**, *8*, No. 14837.
(5) Mannermaa, E.; Vellonen, K.-S.; Urtti, A. Drug transport in corneal epithelium and blood−retina barrier: emerging role of transporters in ocular pharmacokinetics. *Adv. Drug Delivery Rev.* **2006**, *58*, 1136−1163.
(6) SALMINEN, L. Review: Systemic absorption of topically applied ocular drugs in humans. *J. Ocular Pharmacol. Ther.* **1990**, *6*, 243−249.
(7) Jamaledin, R.; Yiu, C. K.; Zare, E. N.; et al. Advances in antimicrobial microneedle patches for combating infections. *Adv. Mater.* **2020**, *32*, No. 2002129.
(8) Li, W.; Terry, R. N.; Tang, J.; et al. Rapidly separable microneedle patch for the sustained release of a contraceptive. *Nat. Biomed. Eng.* **2019**, *3*, 220−229.
(9) Lee, Y.; Kang, T.; Cho, H. R.; et al. Localized delivery of theranostic nanoparticles and high-energy photons using microneedles-on-bioelectronics. *Adv. Mater.* **2021**, *33*, No. 2100425.
(10) Tran, K. T. M.; Gavitt, T. D.; Farrell, N. J.; et al. Transdermal microneedles for the programmable burst release of multiple vaccine payloads. *Nat. Biomed. Eng.* **2021**, *5*, 998−1007.
(11) Than, A.; Liu, C.; Chang, H.; et al. Self-implantable double-layered micro-drug-reservoirs for efficient and controlled ocular drug delivery. *Nat. Commun.* **2018**, *9*, No. 4433.
(12) Park, W.; Nguyen, V. P.; Jeon, Y.; et al. Biodegradable silicon nanoneedles for ocular drug delivery. *Sci. Adv.* **2022**, *8*, No. eabn1772.
(13) Chiappini, C.; Chen, Y.; Aslanoglou, S.; et al. Tutorial: using nanoneedles for intracellular delivery. *Nat. Protoc.* **2021**, *16*, 4539−4563.
(14) Gopal, S.; Chiappini, C.; Penders, J.; et al. Porous silicon nanoneedles modulate endocytosis to deliver biological payloads. *Adv. Mater.* **2019**, *31*, No. 1806788.
(15) Peng, Y.; Tang, L.; Zhou, Y. Subretinal injection: a review on the novel route of therapeutic delivery for vitreoretinal diseases. *Ophthal. Res.* **2017**, *58*, 217−226.
(16) Joussen, A. M.; Wolf, S.; Kaiser, P. K.; et al. The Developing Regorafenib Eye drops for neovascular Age-related Macular degeneration (DREAM) study: an open-label phase II trial. *Br. J. Clin. Pharmacol.* **2019**, *85*, 347−355.
(17) Ferrara, N.; Damico, L.; Shams, N.; Lowman, H.; Kim, R. Development of ranibizumab, an anti−vascular endothelial growth factor antigen binding fragment, as therapy for neovascular age-related macular degeneration. *Retina* **2006**, *26*, 859−870.
(18) Bakri, S. J.; Snyder, M. R.; Reid, J. M.; Pulido, J. S.; Singh, R. J. Pharmacokinetics of intravitreal bevacizumab (Avastin). *Ophthalmology* **2007**, *114*, 855−859.
(19) Bakri, S. J.; Snyder, M. R.; Reid, J. M.; et al. Pharmacokinetics of intravitreal ranibizumab (Lucentis). *Ophthalmology* **2007**, *114*, 2179−2182.
(20) Gaudreault, J.; FEI, D.; BEYER, J. C.; et al. Pharmacokinetics and retinal distribution of ranibizumab, a humanized antibody fragment directed against VEGF-A, following intravitreal administration in rabbits. *Retina* **2007**, *27*, 1260−1266.
(21) Kim, H. M.; Woo, S. J. Ocular drug delivery to the retina: current innovations and future perspectives. *Pharmaceutics* **2021**, *13*, 108.
(22) Holz, F. G.; Tadayoni, R.; Beatty, S.; et al. Multi-country real-life experience of anti-vascular endothelial growth factor therapy for wet age-related macular degeneration. *Br. J. Ophthalmol.* **2015**, *99*, 220−226.
(23) Gillies, M. C.; et al. Long-term outcomes of treatment of neovascular age-related macular degeneration: data from an observational study. *Ophthalmology* **2015**, *122* (9), 1837−1845.
(24) Lu, Y.; Brommer, B.; Tian, X.; et al. Reprogramming to recover youthful epigenetic information and restore vision. *Nature* **2020**, *588*, 124−129.
(25) Peynshaert, K.; Vanluchene, H.; De Clerck, K.; et al. ICG-mediated photodisruption of the inner limiting membrane enhances retinal drug delivery. *J. Controlled Release* **2022**, *349*, 315−326.
(26) Dalkara, D.; Kolstad, K. D.; Caporale, N.; et al. Inner limiting membrane barriers to AAV-mediated retinal transduction from the vitreous. *Mol. Ther.* **2009**, *17*, 2096−2102.
(27) Takahashi, K.; Igarashi, T.; Miyake, K.; et al. Improved intravitreal AAV-mediated inner retinal gene transduction after surgical internal limiting membrane peeling in cynomolgus monkeys. *Mol. Ther.* **2017**, *25*, 296−302.
(28) Candiello, J.; Cole, G. J.; Halfter, W. Age-dependent changes in the structure, composition and biophysical properties of a human basement membrane. *Matrix Biol.* **2010**, *29*, 402−410.
(29) Campochiaro, P. A.; Avery, R.; Brown, D. M.; et al. Gene therapy for neovascular age-related macular degeneration by subretinal delivery of RGX-314: a phase 1/2a dose-escalation study. *Lancet* **2024**, *403*, 1563−1573.
(30) Kim, H.; Jang, H.; Kim, B.; et al. Flexible elastomer patch with vertical silicon nanoneedles for intracellular and intratissue nano-injection of biomolecules. *Sci. Adv.* **2018**, *4*, No. eaau6972.
(31) Hwang, S.-W.; Tao, H.; Kim, D. H.; et al. A physically transient form of silicon electronics. *Science* **2012**, *337*, 1640−1644.
(32) Yin, L.; Farimani, A. B.; Min, K.; et al. Mechanisms for hydrolysis of silicon nanomembranes as used in bioresorbable electronics. *Adv. Mater.* **2015**, *27*, 1857−1864.
(33) Kang, S.-K.; Murphy, R. K. J.; Hwang, S. W.; et al. Bioresorbable silicon electronic sensors for the brain. *Nature* **2016**, *530*, 71−76.
(34) Li, Y.; Zhang, W.; Nguyen, V. P.; et al. Real-time OCT guidance and multimodal imaging monitoring of subretinal injection induced choroidal neovascularization in rabbit eyes. *Exp. Eye Res.* **2019**, *186*, No. 107714.
(35) Qiu, G.; Stewart, J. M.; Sadda, S.; et al. A new model of experimental subretinal neovascularization in the rabbit. *Exp. Eye Res.* **2006**, *83*, 141−152.
(36) Nguyen, V. P.; Henry, J.; Zhe, J.; et al. Multimodal imaging of laser-induced choroidal neovascularization in pigmented rabbits. *Sci. Rep.* **2023**, *13*, No. 8396.
(37) Nguyen, V. P.; Hu, J.; Zhe, J.; et al. Multimodal photoacoustic microscopy, optical coherence tomography, and fluorescence imaging of USH2A knockout rabbits. *Sci. Rep.* **2023**, *13*, No. 22071.
(38) Van Phuc Nguyen, W. Q.; et al. Renally Clearable Ultraminiature Chain-Like Gold Nanoparticle Clusters for Multimodal Molecular Imaging of Choroidal Neovascularization. *Adv. Mater.* **2023**, *35* (31), No. 2302069.
(39) Nguyen, V. P.; Karoukis, A. J.; Hu, J.; et al. Selective nanosecond laser removal of retinal pigment epithelium for cell therapy. *Sci. Rep.* **2024**, *14*, No. 19457.
(40) Nguyen, V. P.; Karoukis, A. J.; Qian, W.; et al. Multimodal Imaging-Guided Stem Cell Ocular Treatment. *ACS Nano* **2024**, *18* (23), 14893−14906.
(41) Nguyen, V.-P.; Li, Y.; Henry, J.; et al. Gold nanorod enhanced photoacoustic microscopy and optical coherence tomography of choroidal neovascularization. *ACS Appl. Mater. Interfaces* **2021**, *13*, 40214−40228.
(42) Nguyen, V. P.; Fan, W.; Zhu, T.; et al. Long-term, noninvasive in vivo tracking of progenitor cells using multimodality photoacoustic, optical coherence tomography, and fluorescence imaging. *ACS Nano* **2021**, *15*, 13289−13306.
(43) Nguyen, V. P.; Paulus, Y. M. Photoacoustic ophthalmoscopy: Principle, application, and future directions. *J. Imaging* **2018**, *4*, 149.
(44) Tian, C.; Zhang, W.; Mordovanakis, A.; Wang, X.; Paulus, Y. M. Noninvasive chorioretinal imaging in living rabbits using integrated photoacoustic microscopy and optical coherence tomography. *Opt. Express* **2017**, *25*, 15947−15955.

https://doi.org/10.1021/acsbiomaterials.5c01783
ACS Biomater. Sci. Eng. 2026, 12, 1269−1285

(45) Weber, J.; Beard, P. C.; Bohndiek, S. E. Contrast agents for molecular photoacoustic imaging. *Nat. Methods* **2016**, *13*, 639−650.
(46) Jathoul, A. P.; Laufer, J.; Ogunlade, O.; et al. Deep in vivo photoacoustic imaging of mammalian tissues using a tyrosinase-based genetic reporter. *Nat. Photonics* **2015**, *9*, 239−246.
(47) Sauvage, F.; Nguyen, V. P.; Li, Y.; et al. Laser-induced nanobubbles safely ablate vitreous opacities in vivo. *Nature Nanotechnol.* **2022**, *17*, 552−559.
(48) Nguyen, V. P.; Li, Y.; Henry, J.; et al. In vivo subretinal ARPE-19 cell tracking using indocyanine green contrast-enhanced multimodality photoacoustic microscopy, optical coherence tomography, and fluorescence imaging for regenerative medicine. *Transl. Vision Sci. Technol.* **2021**, *10*, 10.
(49) Nguyen, V. P.; Li, Y.; Zhang, W.; Wang, X.; Paulus, Y. M. High-resolution multimodal photoacoustic microscopy and optical coherence tomography image-guided laser induced branch retinal vein occlusion in living rabbits. *Sci. Rep.* **2019**, *9*, No. 10560.
(50) Keating, S. C.; Thomas, A. A.; Flecknell, P. A.; Leach, M. C. Evaluation of EMLA cream for preventing pain during tattooing of rabbits: changes in physiological, behavioural and facial expression responses. *PLoS One* **2012**, *7* (9), No. e44437.

https://doi.org/10.1021/acsbiomaterials.5c01783
ACS Biomater. Sci. Eng. 2026, 12, 1269−1285